

A Three Dimensional Gas-Kinetic Scheme with Moving Mesh for Low-Speed Viscous Flow Computations

Changqiu Jin^{1,*}, Kun Xu² and Songze Chen³

¹ *Institute of Applied Physics and Computational Mathematics, Beijing 100088, China*

² *Mathematics Department, Hong Kong University of Science and Technology, Clear Water Bay, Kowloon, Hong Kong*

³ *College of Engineering, Peking University, Beijing 100871, China*

Received 20 December 2009; Accepted (in revised version) 9 May 2010

Available online 26 August 2010

Abstract. The paper introduces the gas-kinetic scheme for three-dimensional (3D) flow simulation. First, under a unified coordinate transformation, the 3D gas-kinetic BGK equation is transformed into a computational space with arbitrary mesh moving velocity. Second, based on the Chapman-Enskog expansion of the kinetic equation, a local solution of gas distribution function is constructed and used in a finite volume scheme. As a result, a Navier-Stokes flow solver is developed for the low speed flow computation with dynamical mesh movement. Several test cases are used to validate the 3D gas-kinetic method. The first example is a 3D cavity flow with up-moving boundary at Reynolds number 3200, where the periodic solutions are compared with the experimental measurements. Then, the flow evolution inside a rotating 3D cavity is simulated with the moving mesh method, where the solution differences between 2D and 3D simulation are explicitly presented. Finally, the scheme is applied to the falling plate study, where the unsteady plate tumbling motion inside water tank has been studied and compared with the experimental measurements.

AMS subject classifications: 76D05

Key words: Gas-Kinetic scheme, moving mesh, low-speed viscous flow, freely moving body.

1 Introduction

There are two different coordinate system for description of fluid motion: the Eulerian one describes fluid motion at fixed locations, and the Lagrangian one follows

*Corresponding author.

URL: <http://www.math.ust.hk/~makxu/>

Email: jin_changqiu@iapcm.ac.cn (C. Q. Jin), makxu@ust.hk (K. Xu), jacksonsze@tom.com (S. Z. Chen)

fluid elements. Considerable progress has been made over the past two decades on developing computational fluid dynamics (CFD) methods based on the above two coordinates system. As the unsteady flow calculations with moving boundaries and interfaces become important, such as found in the flutter simulation of wings, turbomachinery blades, and multiphase flow, the development of fast and reliable methods for dynamically deforming computational domain is required [16].

There are many moving mesh methods in the literature. One example is the static mesh movement method, where the new mesh is generated at each time step according to certain monitor function and the flow variables are interpolated into the newly generated mesh. Then, the flow update through the cell interface fluxes is done on a static mesh. In order to increase the accuracy, the mesh can be properly adapted [5,8]. Another example is the dynamical one, where the mesh is moving according to certain velocity. At the same time, the fluid variables are updated inside each moving control volume within a time step. The second method is mostly used to track the interface location [14], to account for changes in the interface topology, and to resolve small-scale structure at singular point. The most famous one for this dynamical mesh moving method is the Lagrangian method. Through the research in the past decades, it has been well recognized that the Lagrangian method is always associated with the mesh tangling once the fluid velocity is used as the mesh moving velocity. In order to avoid severe mesh distortion in the Lagrangian method, many techniques have been developed. The widely used one at present time is the Arbitrary Lagrangian-Eulerian (ALE) technique, which uses continuous re-zoning and re-mapping from Lagrangian to the Eulerian grid. This process requires interpolations of geometry and flow variables once the computational grid is getting too distorted [13].

Recently, a successful moving mesh method for inviscid Euler equations has been developed by Hui et al. on the target of crisp capturing of slip line [9]. In this unified coordinate method, with a prescribed grid velocity, the inviscid flow equations are written in a conservative form in the computational domain (λ, ξ, η) , as well as the geometric conservation laws which control the mesh deformation. The most distinguishable merit in the unified coordinate method [9] is that the fluid equations and geometric evolution equations are written in a combined system, which is different from the fluid equations alone [5, 10]. Furthermore, due to the coupling of the fluid and geometric system, for the first time the multidimensional Lagrangian gas dynamic equations have been written in a conservative form. As a consequence, theoretically it has been shown that the multidimensional Lagrangian system is only weakly hyperbolic. The distinguishable achievement of the unified coordinate method is that the numerical diffusion across the slip line can be reduced to a minimum level with the crisp capturing of contact discontinuity. However, in the complicated flow movement, in order to avoid the severe mesh distortion, the constraints, such as keeping mesh orthogonality and grid angles, have to be used in the unified coordinate system. As a result, in most cases, the constraint automatically enforces the mesh velocity being zero, such as in the case of gas implosion inside a square. Otherwise, for flow problems with circulations, any mesh movement method, once the grid speed is coupled

with the fluid velocity, will distort the mesh eventually and stop the computation.

Based on the gas-kinetic Boltzmann equation, the Navier-Stokes equations can be derived using the Chapman-Enskog expansion [4]. In the gas-kinetic representation, all macroscopic flow variables are the moments of a single particle distribution function and the particle movement is basically the linear transport and collision. The gas-kinetic BGK scheme has been well developed for the compressible Navier-Stokes solutions [19], and the scheme is especially accurate for the supersonic viscous and heat conducting flow [18, 20]. In the gas-kinetic approach, the gas distribution function is a scalar function, and the particles are moving straightly in all inertia moving reference of frame. Therefore, with the unified coordinate transformation with mesh velocity, the kinetic equation can still keep a simple form. As a continuation of our previous work for the 2D unified coordinate method [12], in this paper a 3D gas-kinetic moving mesh method will be developed. Since the inviscid and viscous fluxes are included simultaneously in the gas-kinetic formulation, the Navier-Stokes fluxes are obtained automatically across the moving cell interface. The focus of this paper is not on the design of mesh moving velocity, but about the construction of gas-kinetic scheme once the mesh moving velocity is given.

This paper is organized as the following. Section 2 is about the mathematical formulation of the 3D gas-kinetic BGK model under the unified coordinate transformation and the construction of the gas-kinetic scheme. Section 3 is about the numerical experiments. The last section is the conclusions.

2 A 3D gas-kinetic BGK scheme with moving mesh

2.1 Gas-kinetic BGK model under unified coordinate transformation

The BGK model of the approximate Boltzmann equation in three-dimensional space can be written as [3]

$$f_t + uf_x + vf_y + wf_z = \frac{g - f}{\tau}, \quad (2.1)$$

where f is the gas distribution function and g is the equilibrium state approached by f . Both f and g are functions of space (x, y, z) , time t , particle velocity (u, v, w) and internal variable ζ . The particle collision time τ is related to the viscosity and heat conduction coefficients. The unified coordinate transformation, i.e., presented in [10, 11], connects the physical domain (t, x, y, z) with the computational domain $(\lambda, \xi, \eta, \zeta)$ through

$$\begin{cases} dt = d\lambda, \\ dx = U_g d\lambda + Ad\xi + Ld\eta + Od\zeta, \\ dy = V_g d\lambda + Bd\xi + Md\eta + Pd\zeta, \\ dz = W_g d\lambda + Cd\xi + Nd\eta + Qd\zeta, \end{cases} \quad (2.2)$$

where (U_g, V_g, W_g) is the grid velocity and $(A, B, C, L, M, N, O, P, Q)$, which is defined by

$$\begin{pmatrix} A & L & P \\ B & M & Q \\ C & N & R \end{pmatrix} = \begin{pmatrix} x_\xi & x_\eta & x_\zeta \\ y_\xi & y_\eta & y_\zeta \\ z_\xi & z_\eta & z_\zeta \end{pmatrix}.$$

With the above transformation (2.2), the 3D gas-kinetic BGK Eq. (2.1) becomes

$$\begin{aligned} \frac{\partial}{\partial \lambda}(\Delta f) + \frac{\partial}{\partial \xi} \{ & [(u - U_g)(MR - QN) + (v - V_g)(PN - LR) \\ & + (w - W_g)(LQ - PM)]f \} + \frac{\partial}{\partial \eta} \{ & [(u - U_g)(QC - BR) \\ & + (v - V_g)(AR - PC) + (w - W_g)(PB - AQ)]f \} \\ + \frac{\partial}{\partial \zeta} \{ & [(u - U_g)(BN - MC) + (v - V_g)(LC - AN) \\ & + (w - W_g)(AM - LB)]f \} = \frac{g - f}{\tau} \Delta, \end{aligned} \tag{2.3}$$

where Δ is the Jacobian of the transformation (2.2) and is defined by

$$\Delta = \det \begin{pmatrix} A & L & P \\ B & M & Q \\ C & N & R \end{pmatrix} = AMR - AQN - BLR + BPN + CLQ - CPM.$$

The inverse transformation is given by

$$\begin{pmatrix} d\lambda \\ d\xi \\ d\eta \\ d\zeta \end{pmatrix} = \begin{pmatrix} 1 & 0 & 0 & 0 \\ \xi_t & \xi_x & \xi_y & \xi_z \\ \eta_t & \eta_x & \eta_y & \eta_z \\ \zeta_t & \zeta_x & \zeta_y & \zeta_z \end{pmatrix} \begin{pmatrix} dt \\ dx \\ dy \\ dz \end{pmatrix}, \tag{2.4}$$

where

$$\begin{pmatrix} 1 & 0 & 0 & 0 \\ \xi_t & \xi_x & \xi_y & \xi_z \\ \eta_t & \eta_x & \eta_y & \eta_z \\ \zeta_t & \zeta_x & \zeta_y & \zeta_z \end{pmatrix} = \frac{1}{\Delta} \begin{pmatrix} \Delta \\ -[U_g(MR - QN) + V_g(PN - LR) + W_g(LQ - PM)] \\ -[U_g(QC - BR) + V_g(AR - PC) + W_g(PB - AQ)] \\ -[U_g(MC - BN) + V_g(AN - LC) + W_g(LB - AM)] \\ 0 & 0 & 0 \\ MR - QN & PN - LR & LQ - PM \\ QC - BR & AR - PC & PB - AQ \\ BN - MC & LC - AN & AM - LB \end{pmatrix}.$$

For an equilibrium flow with distribution $f = g$, by taking the conservative moments

$$\phi = \left(1, u, v, w, \frac{1}{2}(u^2 + v^2 + w^2 + \zeta^2) \right)^T,$$

to Eq. (2.3) and using the above inverse matrix, the corresponding Euler equations under the unified transformation in the Eulerian space can be obtained

$$\frac{\partial E}{\partial \lambda} + \frac{\partial F}{\partial \xi} + \frac{\partial G}{\partial \eta} + \frac{\partial H}{\partial \zeta} = 0, \quad (2.5)$$

where

$$E = \begin{pmatrix} \rho \Delta \\ \rho \Delta U \\ \rho \Delta V \\ \rho \Delta W \\ \rho \Delta E \end{pmatrix}, \quad F = \begin{pmatrix} \rho(I - I_g) \\ \rho U(I - I_g) + p(MR - QN) \\ \rho V(I - I_g) + p(PN - LR) \\ \rho W(I - I_g) + p(LQ - PM) \\ \rho E(I - I_g) + p[U_g(MR - QN) \\ + V_g(PN - LR) + W_g(LQ - PM)] \end{pmatrix},$$

$$G = \begin{pmatrix} \rho(J - J_g) \\ \rho U(J - J_g) + p(QC - BR) \\ \rho V(J - J_g) + p(AR - PC) \\ \rho W(J - J_g) + p(PB - AQ) \\ \rho E(J - J_g) + p[U_g(QC - BR) \\ + V_g(AR - PC) + W_g(PB - AQ)] \end{pmatrix},$$

$$H = \begin{pmatrix} \rho(K - K_g) \\ \rho U(K - K_g) + p(BN - MC) \\ \rho V(K - K_g) + p(LC - AN) \\ \rho W(K - K_g) + p(AM - LB) \\ \rho E(K - K_g) + p[U_g(MC - BN) \\ + V_g(AN - LC) + W_g(LB - AM)] \end{pmatrix},$$

where U , V and W are fluid velocity in the x -, y - and z -directions, and

$$\begin{aligned} I &= U(MR - QN) + V(PN - LR) + W(LQ - PM), \\ J &= U(QC - BR) + V(AR - PC) + W(PB - AQ), \\ K &= U(MC - BN) + V(AN - LC) + W(LB - AM), \\ I_g &= U_g(MR - QN) + V_g(PN - LR) + W_g(LQ - PM), \\ J_g &= U_g(QC - BR) + V_g(AR - PC) + W_g(PB - AQ), \\ K_g &= U_g(MC - BN) + V_g(AN - LC) + W_g(LB - AM). \end{aligned}$$

For the viscous and heat conducting flow, the Chapman-Enskog expansion of Eq. (2.3) gives

$$\begin{aligned} f = g - \frac{\tau}{\Delta} \left\{ \frac{\partial \Delta g}{\partial \lambda} + \frac{\partial}{\partial \xi} \left\{ [(u - U_g)(MR - QN) + (v - V_g)(PN - LR) \right. \right. \\ \left. \left. + (w - W_g)(LQ - PM)] g \right\} + \frac{\partial}{\partial \eta} \left\{ [(u - U_g)(QC - BR) \right. \right. \\ \left. \left. + (v - V_g)(AR - PC) + (w - W_g)(PB - AQ)] g \right\} \right. \\ \left. + \frac{\partial}{\partial \zeta} \left\{ [(u - U_g)(BN - MC) + (v - V_g)(LC - AN) \right. \right. \\ \left. \left. + (w - W_g)(AM - LB)] g \right\} \right\}. \end{aligned}$$

Taking moments ϕ again to Eq. (2.3) with the above gas distribution function, the Navier-Stokes equations with moving meshes can be obtained. Numerically, instead of solving the complicated viscous governing equations, which are similar to those presented in [5], we are going to develop a gas-kinetic scheme based on Eq. (2.3).

2.2 A 3D BGK-NS scheme in a moving mesh system

In this section, we are going to present a 3D gas-kinetic BGK scheme for the viscous solution. For simplification, Eq. (2.3) can be rewritten as

$$\frac{\partial}{\partial \lambda}(\Delta f) + \frac{\partial}{\partial \xi}(S_{\xi} \bar{u} f) + \frac{\partial}{\partial \eta}(S_{\eta} \bar{v} f) + \frac{\partial}{\partial \zeta}(S_{\zeta} \bar{w} f) = \frac{g - f}{\tau} \Delta, \tag{2.6}$$

where Δ is basically a 3D cell volume, S_{ξ} , S_{η} and S_{ζ} are the areas of the faces of the small volume with coordinates $\xi = C_1$, $\eta = C_2$ and $\zeta = C_3$ respectively, which have the following forms

$$\begin{aligned} S_{\xi} &= ((MR - QN)^2 + (PN - LR)^2 + (LQ - PM)^2)^{\frac{1}{2}}, \\ S_{\eta} &= ((QC - BR)^2 + (AR - PC)^2 + (PB - AQ)^2)^{\frac{1}{2}}, \\ S_{\zeta} &= ((BN - MC)^2 + (LC - AN)^2 + (AM - LB)^2)^{\frac{1}{2}}. \end{aligned}$$

Based on the geometrical variables, we can define the normal direction of each interfaces of the control volume, \mathbf{n}_{ξ} , \mathbf{n}_{η} and \mathbf{n}_{ζ} by

$$\begin{aligned} \mathbf{n}_{\xi} &= \frac{\nabla \xi}{|\nabla \xi|} = \frac{(MR - QN, PN - LR, LQ - PM)}{S_{\xi}}, \\ \mathbf{n}_{\eta} &= \frac{\nabla \eta}{|\nabla \eta|} = \frac{(QC - BR, AR - PC, PB - AQ)}{S_{\eta}}, \\ \mathbf{n}_{\zeta} &= \frac{\nabla \zeta}{|\nabla \zeta|} = \frac{(BN - MC, LC - AN, AM - LB)}{S_{\zeta}}. \end{aligned}$$

Therefore, the particle velocity \bar{u} , \bar{v} , \bar{w} in the local coordinates can be expressed as

$$\begin{aligned} \bar{u} &= \mathbf{n}_{\xi} \cdot (u - U_g, v - V_g, w - W_g), \\ \bar{v} &= \mathbf{n}_{\eta} \cdot (u - U_g, v - V_g, w - W_g), \\ \bar{w} &= \mathbf{n}_{\zeta} \cdot (u - U_g, v - V_g, w - W_g). \end{aligned}$$

Obviously, \mathbf{n}_{ξ} , \mathbf{n}_{η} , and \mathbf{n}_{ζ} are perpendicular to the moving planes $\xi = C_1$, $\eta = C_2$ and $\zeta = C_3$, respectively. Then, Eq. (2.6) becomes

$$\frac{\partial}{\partial \lambda}(f) + \frac{\partial}{\partial \bar{x}}(\bar{u} f) + \frac{\partial}{\partial \bar{y}}(\bar{v} f) + \frac{\partial}{\partial \bar{z}}(\bar{w} f) = \frac{g - f}{\tau}, \tag{2.7}$$

where \tilde{x} , \tilde{y} , and \tilde{z} are the physical length in the directions along $\xi = C_1$, $\eta = C_2$ and $\zeta = C_3$. This is the basic equation to be solved in the construction of the local solution f at the point $\xi = C_1$, $\eta = C_2$ and $\zeta = C_3$. Based on the local solution, the corresponding fluxes F , G , and H in different directions can be obtained. In the following, we will present the numerical procedure for computing F . At the same time, both G and H can be obtained similarly.

In order to evaluate the numerical fluxes F across a moving plane $\xi = C_1$ with grid velocity being $\mathbf{q} = (U_g, V_g, W_g)$, we project velocity vector \mathbf{q} on the directions normal to the plane $\xi = C_1$, and tangential to it. Then, we can define orthogonal unit vectors \mathbf{i} , \mathbf{j} , \mathbf{k} , with \mathbf{i} being normal to the moving coordinate plane $\xi = C_1$, i.e.,

$$\mathbf{i} \equiv (i_1, i_2, i_3) = \frac{\nabla \xi}{|\nabla \xi|} = \mathbf{n}_\xi,$$

and \mathbf{j} and \mathbf{k} tangential to it. For example, \mathbf{j} can be chosen arbitrarily on the plane $\xi = \text{constant}$, namely,

$$\mathbf{j} \equiv (j_1, j_2, j_3).$$

Therefore, \mathbf{k} can be defined by

$$\mathbf{k} \equiv (k_1, k_2, k_3) = \mathbf{i} \times \mathbf{j}.$$

Then, the particle velocity $(u - U_g, v - V_g, w - W_g)$ relative to a moving plane can be decomposed into the normal \tilde{u} , and tangential \tilde{v} and \tilde{w} velocities as well, namely

$$\begin{cases} \tilde{u} = (u - U_g)i_1 + (v - V_g)i_2 + (w - W_g)i_3, \\ \tilde{v} = (u - U_g)j_1 + (v - V_g)j_2 + (w - W_g)j_3, \\ \tilde{w} = (u - U_g)k_1 + (v - V_g)k_2 + (w - W_g)k_3. \end{cases} \quad (2.8)$$

The averaged macroscopic fluid velocity components $(\tilde{U}, \tilde{V}, \tilde{W})$ in $(\mathbf{i}, \mathbf{j}, \mathbf{k})$ directions relative to the moving interface can be obtained from the fluid velocity (U, V, W) of the inertia common (x, y, z) coordinates through the same transformation

$$\begin{cases} \tilde{U} = (U - U_g)i_1 + (V - V_g)i_2 + (W - W_g)i_3, \\ \tilde{V} = (U - U_g)j_1 + (V - V_g)j_2 + (W - W_g)j_3, \\ \tilde{W} = (U - U_g)k_1 + (V - V_g)k_2 + (W - W_g)k_3. \end{cases}$$

In the local moving frame of reference on the surface $\xi = C_1$, the Maxwellian distribution has the form

$$g = \rho \left(\frac{\lambda}{\pi} \right)^{\frac{K+3}{2}} \exp \left\{ -\lambda [(\tilde{u} - \tilde{U})^2 + (\tilde{v} - \tilde{V})^2 + (\tilde{w} - \tilde{W})^2 + \zeta^2] \right\}.$$

The general solution f of the Eq. (2.7) at a moving plane $\xi = \xi_{i+1/2}$ and time t is

$$\begin{aligned} f(\xi_{i+1/2}, \eta_j, \zeta_k, t, \tilde{u}, \tilde{v}, \tilde{w}, \zeta) &= \frac{1}{\tau} \int_0^t g(\tilde{x}', \tilde{y}', \tilde{z}', t', \tilde{u}, \tilde{v}, \tilde{w}, \zeta) e^{-\frac{t-t'}{\tau}} dt' \\ &+ e^{-\frac{t}{\tau}} f_0(\tilde{x}_{i+1/2} - \tilde{u}t, \tilde{y}_j - \tilde{v}t, \tilde{z}_k - \tilde{w}t), \end{aligned} \quad (2.9)$$

where

$$(\tilde{x}', \tilde{y}', \tilde{z}') = (\tilde{x}_{i+\frac{1}{2}}, \tilde{y}_j, \tilde{z}_k) - (\tilde{u}, \tilde{v}, \tilde{w})(t - t'),$$

is the trajectory of a particle motion relative to the moving plane and f_0 is the initial gas distribution function f at the beginning of each time step ($t = 0$). With the assumption of the discontinuous distribution function f_0 , the scheme based on the above solution will be identical to the multi-dimensional BGK-NS method [20], even though the coordinate $(\lambda, \tilde{x}, \tilde{y}, \tilde{z})$ is moving relative to the stationary system (t, x, y, z) . In the absence of discontinuities and shocks, f can be simplified to

$$f = g_0[1 - \tau(au + bv + cw) + (t - \tau)A], \tag{2.10}$$

where g_0 is a local Maxwellian distribution function located at $(\zeta_{i+1/2}, \eta_j, \zeta_k)$ and a, b, c, A are related to the derivatives of a Maxwellian in space and time, which can be determined in the same way as that in [21].

Numerically, Eq. (2.7) is basically the same equation as the one we have solved before, where $\tilde{u}, \tilde{v}, \tilde{w}$ are the particle velocity, and $\tilde{U}, \tilde{V}, \tilde{W}$ are the macroscopic velocity in the $i, j,$ and k directions. The standard BGK-NS method [20] can be used here to solve Eq. (2.7) to evaluate the time-dependent gas distribution function $f(\zeta_{i+1/2}, \eta_j, \zeta_k, t, \tilde{u}, \tilde{v}, \tilde{w})$ at the cell interface $\zeta = \zeta_{i+1/2}$. The detailed formulation of the multi-dimensional gas-kinetic BGK-NS scheme for the Navier-Stokes solutions is given in [20]. In this paper, we are only interested in low speed flow computations, such as the incompressible ones. For these flows, we can ignore the energy equations. Therefore, standing on the moving plane the mass and momentum fluxes can be explicitly obtained

$$\begin{pmatrix} \mathcal{F}_\rho \\ \mathcal{F}_{\rho\tilde{u}} \\ \mathcal{F}_{\rho\tilde{v}} \\ \mathcal{F}_{\rho\tilde{w}} \end{pmatrix}_{i+\frac{1}{2},j,k} = \int \tilde{u} \begin{pmatrix} 1 \\ \tilde{u} \\ \tilde{v} \\ \tilde{w} \end{pmatrix} f(\zeta_{i+\frac{1}{2}}, \eta_j, \zeta_k, t, \tilde{u}, \tilde{v}, \tilde{w}) d\tilde{u}d\tilde{v}d\tilde{w}. \tag{2.11}$$

Since different numerical cells can move with different mesh velocity, in order to update the flow variables inside each time-dependent computational cell we need to update the conservative variables relative to the common inertia frame of reference, i.e., the so-called Eulerian space. Therefore, we need to transfer the fluxes in Eq. (2.11) in the moving cell interface into the fluxes for the mass and momentum transport in the common inertia frame of reference. In other words, the above obtained gas distribution function $f(\zeta_{i+1/2}, \eta_j, t, \tilde{u}, \tilde{v}, \tilde{w})$ and its mass flux across the moving cell interface $\tilde{u}f(\zeta_{i+1/2}, \eta_j, t, \tilde{u}, \tilde{v}, \tilde{w})$ will carry the mass and momentum $(1, u, v, w)$ defined in the inertia frame of reference. So, the time-dependent numerical flux in the Eulerian space in the \vec{n} direction across the moving cell interface $\zeta = C_1$ should be calculated as

$$\begin{pmatrix} \mathcal{F}_\rho \\ \mathcal{F}_{\rho u} \\ \mathcal{F}_{\rho v} \\ \mathcal{F}_{\rho w} \end{pmatrix}_{i+\frac{1}{2},j,k} = \int S_\zeta \tilde{u} \begin{pmatrix} 1 \\ u \\ v \\ w \end{pmatrix} f(\zeta_{i+}, \eta_j, \zeta_k, t, \tilde{u}, \tilde{v}, \tilde{w}) d\Xi. \tag{2.12}$$

In order to evaluate the above integrals, we need to use the transformation between the particle velocities $(\tilde{u}, \tilde{v}, \tilde{w})$ and (u, v, w) defined in different frame of reference. Based on the transformation (2.8), the relation between (u, v, w) and $(\tilde{u}, \tilde{v}, \tilde{w})$ are

$$\begin{cases} u = U_g + \tilde{u}(j_2k_3 - k_2j_3) - \tilde{v}(i_2k_3 - k_2i_3) + \tilde{w}(i_2j_3 - j_2i_3), \\ v = V_g - \tilde{u}(j_1k_3 - k_1j_3) + \tilde{v}(i_1k_3 - k_1i_3) - \tilde{w}(i_1j_3 - j_1i_3), \\ w = W_g + \tilde{u}(j_1k_2 - k_1j_2) - \tilde{v}(i_1k_2 - k_1i_2) + \tilde{w}(i_1j_2 - j_1i_2). \end{cases} \quad (2.13)$$

Therefore, Eq. (2.11) becomes

$$\begin{pmatrix} \mathcal{F}_\rho \\ \mathcal{F}_\rho u \\ \mathcal{F}_\rho v \\ \mathcal{F}_\rho w \end{pmatrix}_{i+\frac{1}{2},j,k} = S_\zeta \begin{pmatrix} \mathcal{F}_\rho \\ (j_2k_3 - k_2j_3)\mathcal{F}_{\rho\tilde{u}} - (i_2k_3 - k_2i_3)\mathcal{F}_{\rho\tilde{v}} + (i_2j_3 - j_2i_3)\mathcal{F}_{\rho\tilde{w}} + U_g\mathcal{F}_\rho \\ -(j_1k_3 - k_1j_3)\mathcal{F}_{\rho\tilde{u}} + (i_1k_3 - k_1i_3)\mathcal{F}_{\rho\tilde{v}} - (i_1j_3 - j_1i_3)\mathcal{F}_{\rho\tilde{w}} + V_g\mathcal{F}_\rho \\ (j_1k_2 - k_1j_2)\mathcal{F}_{\rho\tilde{u}} - (i_1k_2 - k_1i_2)\mathcal{F}_{\rho\tilde{v}} + (i_1j_2 - j_1i_2)\mathcal{F}_{\rho\tilde{w}} + W_g\mathcal{F}_\rho \end{pmatrix}, \quad (2.14)$$

where $(\mathcal{F}_\rho, \mathcal{F}_{\rho\tilde{u}}, \mathcal{F}_{\rho\tilde{v}}, \mathcal{F}_{\rho\tilde{w}})$ are given in Eq. (2.11). So, the fluxes across the moving cell interface in the Eulerian space are just linear combinations of the fluxes in the moving frame of reference due to their linear transformations. Similarly, the fluxes at the moving interfaces $\eta = C_2$ and $\zeta = C_3$, i.e., \mathbf{G} and \mathbf{H} can be constructed similarly.

With the above fluxes, the flow variables inside each moving control volume can be updated by

$$\begin{aligned} Q_{i,j,k}^{n+1} = & Q_{i,j,k}^n + \frac{1}{\Delta\zeta} \int_{t^n}^{t^{n+1}} (\mathbf{F}_{i-\frac{1}{2},j,k} - \mathbf{F}_{i+\frac{1}{2},j,k}) dt + \frac{1}{\Delta\eta} \int_{t^n}^{t^{n+1}} (\mathbf{G}_{i,j-\frac{1}{2},k} - \mathbf{G}_{i,j+\frac{1}{2},k}) dt \\ & + \frac{1}{\Delta\zeta} \int_{t^n}^{t^{n+1}} (\mathbf{H}_{i,j,k-\frac{1}{2}} - \mathbf{H}_{i,j,k+\frac{1}{2}}) dt, \end{aligned} \quad (2.15)$$

where

$$Q = (\rho\Delta, \rho\Delta U, \rho\Delta V, \rho\Delta W)^T, \quad \mathbf{F} = (\mathcal{F}_\rho, \mathcal{F}_\rho u, \mathcal{F}_\rho v, \mathcal{F}_\rho w)^T,$$

are given in Eq. (2.14), \mathbf{G} fluxes in the η -direction and \mathbf{H} in the ζ -direction.

3 Numerical experiments

In this section, we are going to test the 3D gas-kinetic scheme in a few well-defined cases, from the rotating cavity flow to freely falling plate inside a water tank. In some cases, the experiment measurements are available.

Case 1: Three-dimensional cavity flow

For two-dimensional cavity flows, extensive research has been conducted using traditional different schemes. The fundamental characteristic of the 2-D cavity flow is the emergence of a large primary vortex in the center and two secondary vortices in the lower corners. The values of the stream function and the locations of the centers

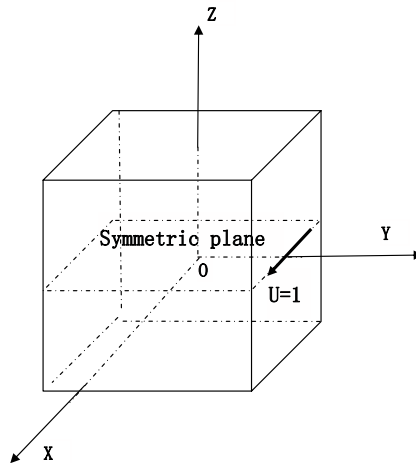


Figure 1: Geometry of the three-dimensional cavity.

of these vortices as a function of Reynolds numbers have been well studied. The gas-kinetic scheme and the lattice Boltzmann simulation of the 2-D driven cavity have been studied [7,21] for a wide range of Reynolds numbers.

In [7], the 3D spatial distributions of the velocity, pressure and vorticity fields were carefully studied. An error analysis of the compressibility effect from the model was carried out. Here, for the first time using the gas-kinetic scheme, a 3D cubic cavity flow is simulated at $Re=3,200$ with $40 \times 40 \times 40$ stretched structure grids. Fig. 1 shows the schematic configuration for the simulation. Flows at this Reynolds number had been extensively studied earlier, including the lattice Boltzmann method [6], the finite-difference simulation and the experimental work [15]. Flow structures, including the velocity fields in different planes, were analyzed using the current method.

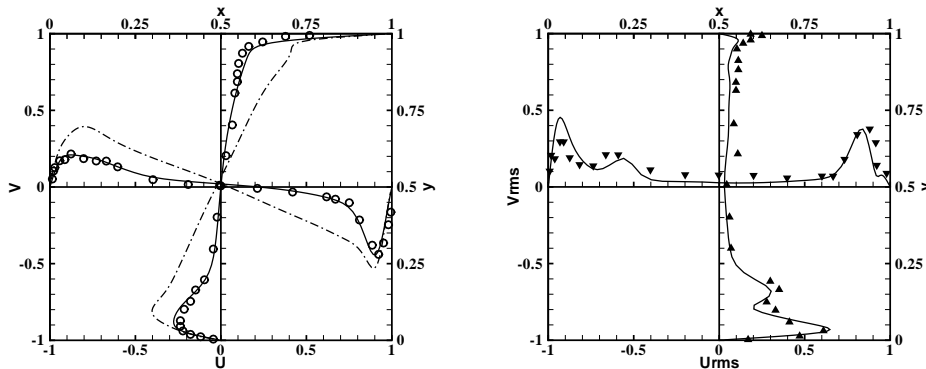


Figure 2: The mean velocity profiles (left), U and V , in the symmetry plane along the vertical and the horizontal centerlines at $Re=3200$. The solid line is the current 3D simulation, the dotted line is the 2D simulation, and the circles represent experimental results [15]. The root-mean-square (rms) velocity profiles (right), i.e., U_{rms} and V_{rms} , are obtained in the symmetry plane along vertical and horizontal centerlines. The solid lines are the current 3D simulation, and upward triangles and downward triangles are experimental measurements [15].

Fig. 2 displays the mean velocity (left) and the root-mean-square (rms) velocity (right) profiles in the symmetry plane along the vertical and the horizontal centerlines, from the current 3D calculation. For a comparison, a 3-D gas-kinetic scheme simulations and the experimental measurements are also presented. The agreement between them shows that the 3D gas-kinetic scheme is capable of simulating complex 3D unsteady flows.

Case 2: The rotating flow inside a 3D cavity

This is the study of the flow inside a cubic box which rotates along an axis in the z -direction. The schematic of the 3D rotating cavity is shown in Fig. 3. The uniform grid is adopted. Initially, the flow inside the box is stationary and has zero fluid velocity. With the start of the rotation of the box at $t = 0$ with an angular velocity $\omega = 1.0$, the fluid starts to move first from the six boundary surfaces due to the viscous stress

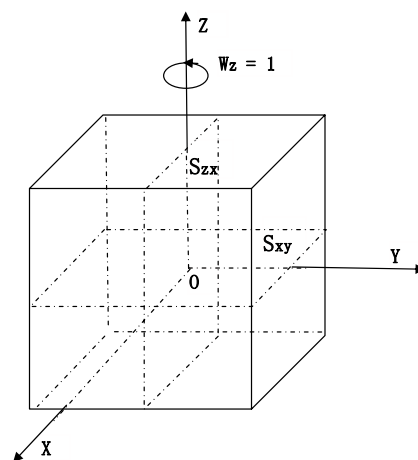


Figure 3: The schematic of three dimensional rotating cavity along z -axis $\omega = \omega_x x + \omega_y y + \omega_z z$, where $\omega_x = \omega_y = 0$ and $\omega_z = 1$.

force from the moving boundary. At times $t = 2\pi$ and 4π , the x -velocity profile at the symmetric plane $z = 0$ along y -axis is shown in Fig. 4. In the same figure, in order to compare the differences between the 2D and 3D solutions due to the additional top and bottom walls in the 3D case, the velocity profile for the 2D calculations is also presented in this figure. As shown in the figure, due to the top and bottom walls of the box, the velocity change in 3D case is larger than that in the 2D case. The streamlines for the (U, V) velocity components inside the symmetric plane $z = 0$ are shown in Fig. 5 for the two times $t = 2\pi$ and 4π . Inside the plane $y = 0$, the corresponding streamlines for the velocity components (U, W) are shown in Fig. 6. The unsteady complicated flow structures are presented.

Case 3: Falling plate simulation

In order to test the accuracy of the 3D code in the capturing of unsteady solution, we are going to simulate the experiment conducted by Andersen, Persavento and Wang [1], where a small rectangular aluminum plate was falling freely in a wa-

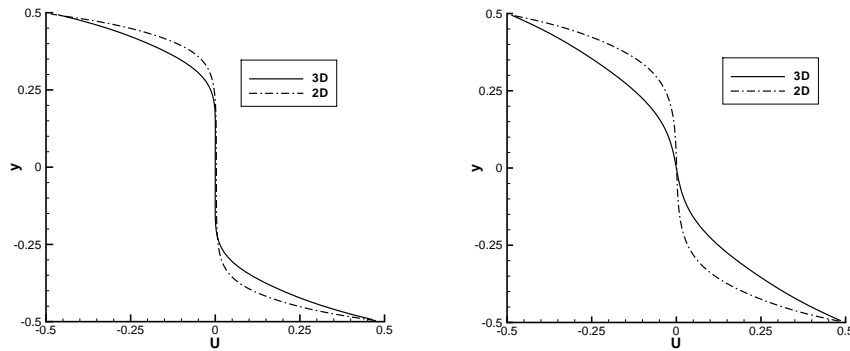


Figure 4: Velocity profile U at Time= 2π (left) and Time= 4π (right), in the symmetry plane along the vertical centerline, with rotating speed $\omega = \omega_x x + \omega_y y + \omega_z z$, where $\omega_x = \omega_y = 0$ and $\omega_z = 1$. The solid line is the current 3D simulation, and the dotted line is the current 2D simulation.

ter tank. In the experiments, for the rectangular plate many physical quantities were measured, such as the plate trajectory and falling speed. The fluid force and torque on the plate were calculated according to the experimental data. Due to the limitation

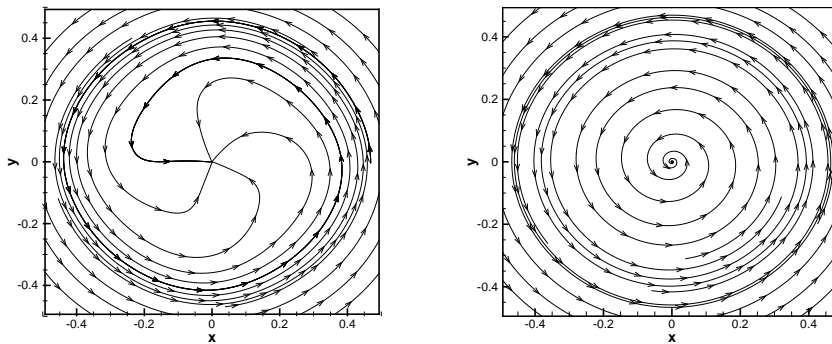


Figure 5: Streamline of velocity (U,V) at Time= 2π (left) and Time= 4π (right), in the symmetry plane, with rotating speed $\omega = \omega_x x + \omega_y y + \omega_z z$, where $\omega_x = \omega_y = 0$ and $\omega_z = 1$.

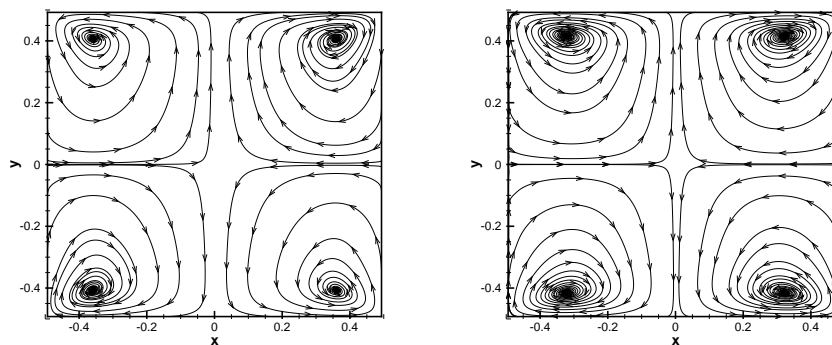


Figure 6: Streamline of velocity (U,W) at Time= 2π (left) and Time= 4π (right), in the xz -plane, with rotating speed $\omega = \omega_x x + \omega_y y + \omega_z z$, where $\omega_x = \omega_y = 0$ and $\omega_z = 1$.

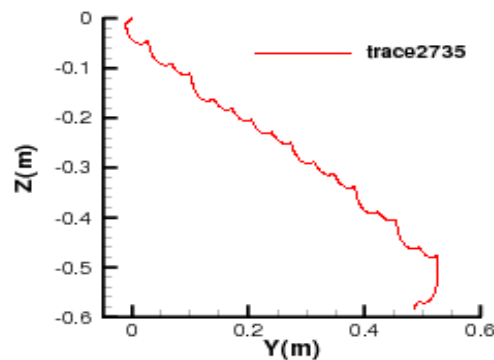


Figure 7: Plate trajectory in the whole simulation.

of the numerical method used in [1], only a 2D simulation for an elliptic plate was presented. Since the experiment is basically a 2D flow, in our study we are going to use the 3D code with a periodic homogeneous flow condition in the 3rd direction in order to recover the 2D experiment.

In our computation, a rectangular cross-section is chosen according to the experimental data [1]. A stretched structure mesh with the mesh size 217×51 is generated around the rectangular plate and an additional 3 mesh points are used in the 3rd direction. The inner boundary of the computational domain is the falling plate surface, and the outer boundary is a cylindrical circle with a radius of 10 times of long axis of the plate. According to the experiments, the thickness-to-length ratio of the cross-section is $\beta = 1/8$, with the plate thickness $h = 8.1 \times 10^{-4}$ m and length $l = 6.48 \times 10^{-3}$ m. The density of fluid is $\rho_f = 1000$ kg/m³ with a dynamical viscosity coefficient $\mu = 8.9 \times 10^{-4}$ kg/m·s. The density of aluminum used in our calculation is $\rho_s = 2735$ kg/m³, which is slightly different from the stated value $\rho_s = 2700$ kg/m³ used in [1]. With the above parameters, the dimensionless moment of inertia of the plate becomes

$$I^* = \frac{8}{3\pi} F_r^2 \left[1 + \left(\frac{h}{l} \right)^{\frac{1}{2}} \right] = 0.2974,$$

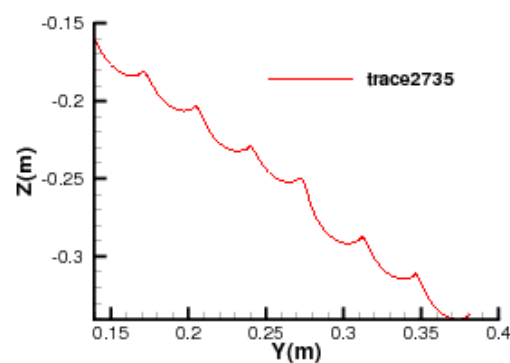


Figure 8: Plate trajectory in the tumbling parts, where two periodic motion can be clearly observed.

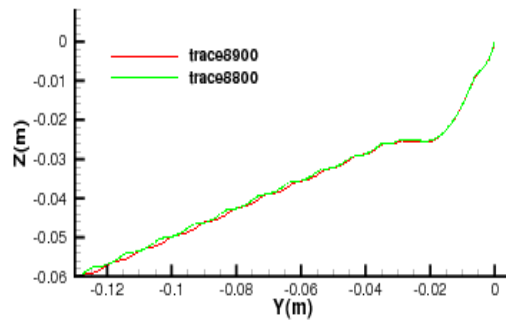


Figure 9: Plate trajectory with tumbling motion only for the plates with densities $\rho_s = 8900 \text{ kg/m}^3$ and $\rho_s = 8800 \text{ kg/m}^3$.

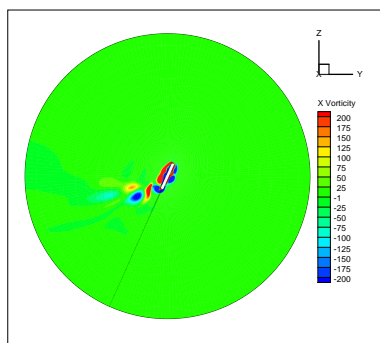


Figure 10: Vortex distribution around the moving plate.

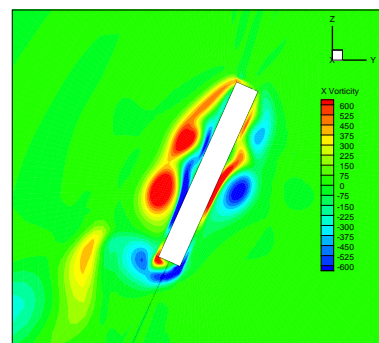


Figure 11: Detailed vortex field around the moving plate.

where the Froude number is defined [2]

$$Fr = \left(\frac{\rho_s h}{\rho_f l} \right)^{\frac{1}{2}}$$

The plate is released from rest at an angle of 45° with respect to the horizontal level. In the simulation, the mesh around the plate is moving with the plate together. In

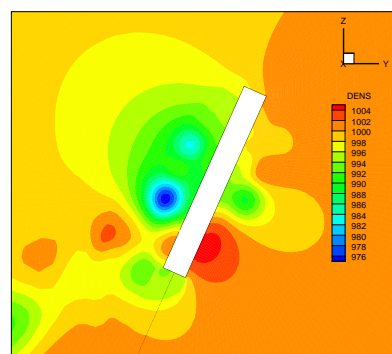


Figure 12: Detailed pressure distributions around the moving plate.

Table 1: Experimental and numerical falling plate averaged translational and angular velocities.

	ρ_s [kg·m ⁻³]	I^*	U_y [m/s]	U_z [m/s]	ω [rad/s]
Experiment	2700	0.29	0.159 ± 0.003	-0.115 ± 0.005	14.5 ± 0.3
Computation	2735	0.2947	0.1596	-0.1158	14.26

the inertia reference of frame, the Cartesian x -axis is defined as the plate span-wise direction, the y -axis is on the horizontal direction and the z -axis is on the vertical direction.

As showed in Fig. 7, the trajectory is not a very stable one. The reason for this phenomenon is that the experiment set-up makes the current plate motion in the transitional regime, where both fluttering and tumbling motion exist. For a rectangular cross-section, the transition regime is determined by the critical value of the parameter I^* . Based on the earlier investigation, the critical value is between 0.2 and 0.3 [17], or 0.39 [2]. The experimental measurement taken by Andersen et al. [1] seems settled in this transitional regime. In addition, the four trajectories presented in [1] confirm the above conjecture. As the parameter I^* changes from 0.16 to 0.48, the plates undergo fluttering, tumbling with double periods structure [1], chaotic, and tumbling motion. Based on a section of the trajectory, see Fig. 8, the averaged quantities derived the computation data match with the experimental data very well, see Table 1. The vorticity and pressure distributions around the plate are shown in Figs. 10, 11 and 12, where a smooth flow distributions can be clearly observed. If we change the plate densities to $\rho_s = 8900 \text{ kg/m}^3$ and $\rho_s = 8800 \text{ kg/m}^3$, the parameters I^* become 0.9591 and 0.9483, where in this regime only tumbling motion exists. Fig. 9 presents the two trajectories which will last forever. The detailed numerical results are listed in Table 2.

In the above computations, we only consider one moving object and the mesh is rigidly attached to the object. As a result, the mesh is moving together with the movement of the single object. At this time, we have difficulties to extend the present formulation to simulate movement of multiple bodies. Theoretically, once the mesh moving velocity is given, the kinetic formulation of the flux evaluation and the update of flow variables in a moving control volume should be the same as the method presented in this paper. Practically, multiple bodies with relative movement will introduce additional difficulties in the mesh generation and the assigning of mesh velocities. Especially, with the structured mesh and fixed mesh points it seems impossible to simulate two freely moving bodies. In order to simulate multiple body movements inside a fluid, instead of physical modeling and the flux evaluation, the computer programming skill and the ability of handling data structure with variable mesh points plays a more important role here.

Table 2: Averaged translational and angular velocities of two periodic stable trajectories.

	ρ_s [kg·m ⁻³]	I^*	U_y [m/s]	U_z [m/s]	ω [rad/s]
Trace88	8800	0.9483	-0.1906	-0.0649	-56.05
Trace89	8900	0.9591	-0.2062	-0.0673	-75.36

4 Conclusions

In this paper, a three-dimensional gas kinetic scheme with moving mesh is presented for the low-speed viscous flow computation. The scheme is validated in a few test cases, where the computational solutions match with the experimental measurements very well. The simplicity of the gas-kinetic scheme with moving mesh is solely based on the simple physical mechanism of particle transport and collisions, which is the same in both x - y - z coordinate system and the local moving ones. Also, due to the kinetic formulation, a low-speed viscous flow solver can be constructed easily. Otherwise, the macroscopic Navier-Stokes equations under the general coordinate transformation are extremely complicated [5] and its direct numerical discretization becomes very difficult. The main purpose of this paper is not to present any idea about how to construct an optimal mesh velocity in the flow simulation. Instead, for a given mesh velocity, an accurate gas-kinetic scheme for the Navier-Stokes equations is presented for three-dimensional flow simulation.

Acknowledgments

The work described in this paper was substantially supported by grants from the National Natural Science Foundation of China (Project No.10772033). K. Xu was supported by Hong Kong Research Grant Council 621709.

References

- [1] A. ANDERSEN, U. PERSAVENTO AND Z. JANE WANG, *Unsteady aerodynamics of fluttering and tumbling plates*, J. Fluid. Mech., 541 (2005), pp. 65–90.
- [2] A. BELMONTE, H. EISENBERG AND E. MOSES, *From flutter to tumble: inertial drag and froude similarity in falling paper*, Phys. Rev. Lett., 81 (1998), pp. 345–348.
- [3] P. L. BHATNAGAR, E. P. GROSS AND M. KROOK, *A model for collision processes in gases I: small amplitude processes in charged and neutral one-component systems*, Phys. Rev., 94 (1954), pp. 511–525.
- [4] S. CHAPMAN AND T. G. COWLING, *The Mathematical Theory of Non-Uniform Gases*, Cambridge University Press, 1990.
- [5] K. A. HOFFMANN AND S. T. CHIANG, *Computational fluid dynamics for engineers*, third edition, 2 (1993), pp. 21–46, published by Engineering Education System, Wichita, Kansas.
- [6] S. HOU, *Lattice Boltzmann Method for Incompressible Viscous Flow*, PhD thesis, Kansas State University, Manhattan, Kansas, 1995.
- [7] S. HOU, Q. ZOU, S. CHEN, G. DOOLEN AND A. C. COGLEY, *Simulation of cavity flow by the lattice Boltzmann method*, J. Comp. Phys., 118 (1995), pp. 329–347.
- [8] W. HUANG, *Mathematical principles of anisotropic mesh adaptation*, Commun. Comput. Phys., 1 (2006), pp. 276–310.
- [9] W. H. HUI, P. Y. LI AND Z. W. LI, *A unified coordinate system for solving the two-dimensional Euler equations*, J. Comput. Phys., 153 (1999), pp. 596–637.

- [10] W. H. HUI AND G. P. ZHAO, *Capturing contact discontinuities using the unified coordinates*, Proceedings of Second MIT Conference on Computational Fluid and Solid Mechanics, 2003, pp. 2000–2003.
- [11] W. H. HUI AND S. KUDRIAKOV, *A unified coordinate system for solving the three-dimensional Euler equations*, J. Comput. Phys., 172 (2001), pp. 235–260.
- [12] C. Q. JIN AND K. XU, *A unified moving grid gas-kinetic method in Eulerian space for viscous flow computation*, J. Comput. Phys., 222 (2007), pp. 155–175.
- [13] K. LIPNIKOV AND M. SHASHKOV, *The error minimization based strategy for moving mesh methods*, Commun. Comput. Phys., 1 (2006), pp. 53–80.
- [14] H. LUO, J. D. BAUM AND R. LOHNER, *On the computation of multi-material flows using ALE formulation*, J. Comput. Phys., 194 (2004), pp. 304–328.
- [15] A. K. PRASAD AND J. R. KOSEFF, *Reynolds-number and end-wall effects on a lid-driven cavity flows*, Phys. Fluids. A., 1 (1989), pp. 208–225.
- [16] W. SHYY, H. S. UDAYKUMAR, M. M. RAO AND R. W. SMITH, *Computational Fluid Dynamics with Moving Boundaries*, Taylor and Francis, Washington DC, 1996.
- [17] E. H. SMITH, *Autorotating wings: an experimental investigation*, J. Fluid. Mech., 50 (1971), pp. 513–534.
- [18] M. SUN, T. SAITO, P. A. JACOBS, E. V. TIMOFEEV, K. OHTANI AND K. TAKAYAMA, *Axially asymmetric shock wave interaction with a cone: a benchmark test*, Shock. Waves., 14 (5–6) (2003), pp. 313–331.
- [19] K. XU, *A gas-kinetic BGK scheme for the Navier-Stokes equations and its connection with artificial dissipation and Godunov method*, J. Comput. Phys., 171 (2001), pp. 289–335.
- [20] K. XU AND M. L. MAO, *A multidimensional gas-kinetic BGK scheme for hypersonic viscous flow*, J. Comput. Phys., 203 (2005), pp. 405–421.
- [21] K. XU AND X. HE, *Lattice Boltzmann method and gas-kinetic BGK scheme in the low-Mach number viscous flow simulations*, J. Comput. Phys., 190 (2003), pp. 100–117.